

The stability of AdS

Jorge Daniel Casaleiro Lopes

Thesis to obtain the Master of Science Degree in

Engineering Physics

Supervisor: Prof. Vitor Manuel dos Santos Cardoso
Dr. Hirotada Okawa

Examination Committee

Chairperson: Prof. José Pizarro de Sande e Lemos
Supervisor: Dr. Hirotada Okawa
Members of the Committee: Prof. Amaro Jose Rica da Silva
Dr. Jorge Miguel Cruz Pereira Varelas da Rocha

October 2014

Acknowledgments

This work would not have been possible without the support of many people. I would like to acknowledge my supervisor, Professor Vitor Cardoso, and my co-supervisor, Dr. Hirotada Okawa, for their guidance and advice during the entire process. I would also like to thank CENTRA research center for receiving me and help for my recent academic development.

The numerical simulations that were performed for this work were partially run in CENTRA's super-computer, Baltasar Seven Suns and in a particular server managed by Duarte Nina. I would like to thank the opportunity to use these machines in this study.

In particular I would also like to thank Inês Almeida for her suggestions while writing this document, to Gonçalo Quintal for his support during the process, specially during the summer, and to Bruno Pereira and the numerical group from IST's mathematical department lead by Prof. Carlos Alves for their suggestions.

I would like to give a special thanks to my friends for their sympathy and my colleges their assistance. Finally, I would like to thank my family for their love and understanding. Your support has been invaluable, for which I am very grateful.

Resumo

O problema da estabilidade de espaços contra a possibilidade de colapso é bastante complexo e fundamental em física teórica. Resultados recentes que indicam que espaços anti-de Sitter são não linearmente instáveis diante da possibilidade da formação de buracos negros desvendam a excitante, embora inconveniente, possibilidade que este fenómeno se revele ser a regra nos fenómenos gravíticos. A instabilidade do espaço anti-de Sitter é, por si só, um resultado notável com importantes consequências na nossa compreensão da dualidade entre teorias de gauge e gravíticas e sobre espaços-tempo sob a influência de uma constante cosmológica. No entanto, é possível que as consequências sejam tão abrangentes que tocam mesmo em temas como a física fundamental e a astrofísica no caso deste colapso ser desencadeado por configurações genéricas nas quais a matéria encontra-se confinada.

O objectivo desta tese é rever e reproduzir o estado da arte da área. A dinâmica presente nas equações de campo e na Relatividade Geral são altamente não lineares e só foram encontradas soluções analíticas para um pequeno conjunto de casos. Logo, o estudo do colapso gravítico em espaços anti-de Sitter é feito através de aproximações numéricas usando o formalismo ADM. Os nossos resultados são compatíveis com resultados apresentados na literatura: dados iniciais genéricos levam ao colapso gravítico. Embora o colapso gravítico possa ser adiado para dados menos intensos, este fenómeno é inevitável. O tamanho x_{BH} do buraco negro formado tem uma dependência complexa na amplitude inicial e é descrita, em certos pontos, pelo comportamento crítico $x_{BH} \propto (\epsilon - \epsilon^*)^\gamma$, apresentado por Choptuik, com constante universal γ .

Palavras-chave: Relatividade Geral, Anti-de Sitter, colapso, buraco negro, campo escalar.

Abstract

The problem of stability of spacetimes against gravitational collapse is a complex but fundamental open problem in theoretical physics. Recent results indicating that anti-de Sitter spacetimes are nonlinearly unstable against the formation of black holes open the exciting, if troublesome possibility that collapse may be the rule rather than the exception in gravitational physics. On its own, the instability of anti-de Sitter is a remarkable result with important consequences for our understanding of the gauge-gravity duality and for spacetimes with a cosmological constant. However, there might be broader consequences for fundamental physics and astrophysics, if gravitational collapse is triggered for "generic" setups where matter is confined.

The purpose of this thesis is to review and reproduce the state of the art in the field. The dynamics encoded in the field equations of General Relativity is highly nonlinear and analytical solutions have been found only for a handful of special cases. We therefore study gravitational collapse in anti-de Sitter spacetimes through a numerical approach using the so-called ADM formalism. Our results are compatible with previous findings in the literature: generic initial data leads to gravitational collapse. Gravitational collapse can be delayed for sufficiently small initial data amplitude, but cannot be avoided. The size x_{BH} of the black hole formed has a complex dependence on initial amplitude and is described, at discrete points, by Choptuik's critical behavior $x_{BH} \propto (\epsilon - \epsilon_*)^\gamma$ with a universal constant γ .

Keywords: General Relativity, anti-de Sitter, gravitational collapse, black hole, gauge/gravity, field theories.

Contents

Acknowledgments	iii
Resumo	v
Abstract	vii
List of Tables	xi
List of Figures	xiii
Nomenclature	xv
1 Introduction	1
1.1 Motivation	2
1.2 State-of-the-art	2
1.3 Original Contributions	9
1.4 Structure of the Thesis	9
2 Theory	11
2.1 Overview of the AdS spacetime	11
2.2 Dynamic model of the AdS spacetime	12
2.2.1 Projections of the Einstein equation	13
2.2.2 The evolution equations	14
3 Numerical Methods and Results	17
3.1 Spatial profiles and Convergence tests	17
3.2 Time evolution	21
3.3 The stability of the AdS spacetime	25
4 Conclusions	29
4.1 Achievements	29
4.2 Future Work	30
Bibliography	32

List of Tables

3.1 Critical points properties 27

List of Figures

1.1	Horizon radius vs amplitude for initial data (Result from Bizoń et al.)	6
3.1	A function as a function of x for initial data	18
3.2	$(R - 1)$ ratio as a function of N	20
3.3	δ function's spatial profile using initial data profile	21
3.4	Π and Φ profile over time using a straight forward second order method	23
3.5	Π and Φ profile over time using a fourth order method	24
3.6	x_{BH} as a function of ϵ	26
3.7	t_{BH} as a function of ϵ	27
3.8	Π^2 as a function of time, for $\epsilon = 7.0$ and $\epsilon = 1.4$	28

Nomenclature

GR	General Relativity
dS	de Sitter
AdS	Anti-de Sitter
CFT	Conformal field theories
ADM	Arnowitt-Deser-Misner
CFL	Courant-Friedrichs-Lewy

Chapter 1

Introduction

The discovery of the AdS/CFT correspondence [27] is an important achievement in modern physics. It allows scientists to relate phenomena that take place in an Anti-de Sitter (AdS) spacetime, a Universe with a negative cosmological constant, with phenomena in Conformal Field theories (CFT), which are field theories invariant to conformal, or angle-preserving, transformations. It was discovered in 1997, by Maldacena [19], and it has attracted the interest of the scientific community ever since. This is a very extensive and complex topic to cover in this work but we can draw some conclusions from our work regarding its consequences in the light of this correspondence. In particular, regarding the thermodynamics of black holes and its consequences for CFT's. This duality has a wide range of applications that covers not only quantum field theories, but also many body theories and condensed matter physics [16, 22], nuclear physics and quantum chromodynamics [8, 10]. For introductory documentation on this topic see [1, 18].

Although the cosmological implications of a negative cosmological constant may be very interesting, there is little evidence that our Universe behaves as such. However, a spacetime with these characteristics allows us to study certain properties of the gravity, in particular when under a confined space. Literature suggests that, in the simplest cases, confined fields under the influence of gravity always collapse and form a black hole. The importance of this result goes beyond the AdS/CFT correspondence, reaching as far as the fundamental behaviour of gravity in General Relativity.

The notion of spacetime as an intrinsically geometric quantity which can be distorted, pushed and thorn apart is nowhere better illustrated than with the notion of black holes. These extreme solutions of Einstein field equations are now known to be abundant objects in the universe, lurking at the center of most galaxies and powering quasars, jets and even the growth of the galaxy itself. Black holes also clothe Einstein's theory own demise: singularities, which are points where tidal forces diverge and quantum effects become important. Quantum effects become important in the regions close to singularities and an improved, yet unknown, theory is required.

The interest in strong field dynamics, in particular concerning black holes, has exponentiated in recent years, triggered by several developments at the technical and conceptual level. Unfortunately, the equations that rule such field's dynamics are non-linear and, because of this, only a set of problems

have been fully solved. Computational techniques have progressed faster and become more robust for the last hundred years and these properties together with their versatility make it a very useful resource to tackle some of the hardest problems in modern physics. Although numerical results do not replace actual theoretical demonstration or experimental data, they can be used to point research in the right direction. In the present work we will use numerical techniques to study a massless scalar field in AdS as cosmological background. The evolution of this field will be computed using GR, or the Einstein equation, and the Klein-Gordon equation.

1.1 Motivation

GR is the relativity theory which includes the effects of gravity as a distortion, or curvature, of the spacetime. Shortly after its formulation in 1915 by Albert Einstein, many cosmological models emerged as solutions of the Einstein equation. Our focus will be to study the systems that have a negative cosmological constant because it can be extended as a solution of the Einstein equation but it can be used to model for other confined, or almost confined, systems such as stars or nebulae during the accretion process. The effect the cosmological constant produces is geometric in nature and, in AdS, it is equivalent to a constant attractive force between any two particles, or a space with positive pressure and negative vacuum energy. This property makes the AdS spacetimes a very interesting framework as fields can reach the conformal spatial infinity in a finite time. Field under such conditions will remain confined in the spacetime, such as stars or black holes. Although we still need to set the appropriate boundary conditions, they come naturally from the model compared to flat spacetimes with imposed artificial boundary conditions such as a mirror at a finite distance.

Our focus is the evolution of fields, or waves, in AdS. We want to understand not only how the fields behave, but also how the spacetime behaves when time-evolving fields are present and how these fields collapse and form structures like stars and, ultimately, black holes. Although there are no direct proof for the existence of black holes, there are several indirect evidence that they exist in nature. Although there is a lot of research done concerning black holes, there are still today a lot of open questions from both the mathematical point of view and a philosophical perspective. These are topics that are not fully understood have a lot of unanswered questions and are outside the scope of this work.

The problem we are going to study in this document consists of a free, or massless, real spherically symmetric scalar field using the AdS spacetime as background. Although this seems a very simplified conceptual model one should understand that numerical relativity is a very recent area of physics not only because of the late growth of computational power but also due to the nature of the equations that describe the systems we are trying to simulate.

1.2 State-of-the-art

In 1992, Choptuik [9] studied the collapse of a scalar field with a general time and radial spatial dependent metric. He considered the simplest case, which uses an ingoing spherically symmetric field.

The evolution equations of the system are obtained using the Einstein equation and the Klein-Gordon equation. Using, as an ansatz, the line element

$$ds^2 = -\alpha^2(r, t)dt^2 + a^2(r, t)dr^2 + r^2 d\Omega^2, \quad (1.1)$$

where α and a are the geometric coefficients and $d\Omega$ is the solid angle of a $D - 2$, or in this particular case, a 2-sphere. With the auxiliary variables $\Phi = \dot{\phi}$ and $\Pi = a\dot{\phi}/\alpha$, the Klein-Gordon and Einstein equations become

$$\dot{\Phi} = \left(\frac{\alpha}{a}\Pi\right)', \quad \dot{\Pi} = \frac{1}{r^2} \left(r^2 \frac{\alpha}{a}\Phi\right)', \quad (1.2)$$

$$\frac{\alpha'}{\alpha} - \frac{a'}{a} + \frac{1 - a^2}{r} = 0, \quad (1.3)$$

$$\frac{a'}{a} + \frac{a^2 - 1}{2r} - 2\pi r (\Pi^2 + \Phi^2) = 0, \quad (1.4)$$

The author used an adaptive mesh-refinement algorithm where the discretization step can vary locally, not only in space but also in time. He studied the collapse for different initial profiles of matter density and concluded that each family of initial data had its own critical point p^* and that all the profile families follow a law of the form

$$M_{BH} \propto |p - p^*|^\gamma, \quad (1.5)$$

where p characterizes the strength of the gravitational self-interaction of the scalar field and γ is a growth parameter and M_{BH} is the mass of the black hole at the time of its formation. Also, in Eq. (1.5), we would expect the p^* and γ parameters to be independent among different families of initial data. In fact, from the results, the author concluded that $\gamma \simeq 0.37$ and that this parameter is the same for all families of initial data, i.e. γ is an universal constant.

In 1996, Gundlach [15] extended Choptuik's work by using a complex, or charged, field. After confirming Choptuik's power law with the critical exponent he studied the influence of a global charge in the black hole collapse. He verified that the charge of the black hole also grows with a power law of the form

$$Q_{BH} \propto |p - p^*|^\delta. \quad (1.6)$$

He also verified the same universal constant, $\gamma = 0.374 \pm 0.001$, as Choptuik and he determined the constant $\delta = 0.883 \pm 0.007$.

Later, in 1999, Garfinkle et al. [12] studied Choptuik's system in six dimensions. For the six dimensional system, Garfinkle et al. obtained $\gamma = 0.424$. Although this does not represent the global tendency of the system, we can see that the universal constant γ is locally growing with the number of dimensions, meaning that the black hole initial mass will grow progressively slower with the dimension of the spacetime.

In 2000, Pretorius and Choptuik [26] studied the previously described scalar field collapse in AdS.

They analysed the nature of the AdS spacetime and verified that the boundary conditions imposed for this problem are the only ones that prevent out-going waves from leaving the Universe through spatial infinity. They verified Choptuik's previous results [9] and confirmed that the waves reach spatial infinity in finite time and it is reflected, making it travel inward afterwards. They concluded that their approach is different from a particle collision or thin dust approach because with these considerations one obtains different exponential factors. Although they recognize and criticize the threshold for the black hole formation, they did not study thoroughly the evolution with fields weaker than the critical point, as we shall note later in this section, leaving it to future work.

In 2003, Dumitru Astefanesei and Eugen Radu [3] studied boson stars in AdS or the dynamics of a complex scalar field in an AdS spacetime. They also used a slightly different Energy-momentum tensor. While most literature uses a massless scalar field ($V(\phi) = 0$), the author of this paper used a mass term $V(\phi) = \mu^2 \phi^* \phi$. With this approach, the self-interacting term $\lambda|\phi|^4$ is neglected. The authors of [3] used the metric¹

$$ds^2 = \frac{dr^2}{F(r)} + r^2 d\Omega_{D-2}^2 - F(r)e^{2\delta(r)} dt^2, \quad (1.7)$$

where

$$F(r) = 1 - \frac{m(r)}{r^{D+3}} - \frac{2\Lambda r^2}{(D-2)(D-1)}. \quad (1.8)$$

They also assumed that the waves could be decomposed in their radial and time components i.e., $\Phi = \phi(r)e^{-i\omega t}$ and, for the particular case of three dimensions, the following relation is obtained

$$(1 - 2m)\phi'^2 + \frac{\omega^2 e^{2\delta} \Lambda r^2}{F^2} \phi^2 = 0. \quad (1.9)$$

The rescaled differential equations for these parameters are

$$m' = \frac{r^{D-2}}{2} \left(F\phi'^2 + \phi^2 + \frac{e^{2\delta}\phi^2}{F} \right), \quad (1.10)$$

$$(e^{-\delta})' = r \left(e^{-\delta}\phi'^2 + e^{\delta}\frac{\phi^2}{F^2} \right), \quad (1.11)$$

$$(r^{D-2}e^{-\delta}F\phi')' = r^{D-2}e^{-\delta}\phi \left(1 - \frac{\phi^2}{F^2} \right). \quad (1.12)$$

With this line element, this decomposition and the appropriate boundary conditions it is possible to solve the above system numerically for $D = 3, 4, 5$ and $\Lambda < 0$.

The authors of [3] concluded that if we increase the influence of the cosmological constant, the maximum star mass and the maximum particle number will slightly decrease. They also concluded that, for a nonzero Λ , the fields vanish at spatial infinity with a power law, instead of a theoretically expected exponential decay for a flat spacetime. Also, one can physically explain the decrease in mass and particle charge. The star's self-gravity decrease is compensated with the cosmological constant's

¹The authors did not use a trigonometric variable transformation, possibly because of the novelty of this topic and the AdS/CFT correspondence at the time.

attractive force, keeping the star's particles bounded.

In 2011, Bizoń and Rostworowski [5] studied the evolution of a spherically symmetric scalar field in an AdS spacetime. This article represents one of the first computational results on dynamics in AdS space using explicitly bound spatial coordinates, in the study of field dynamics in AdS.

The equations that describe the dynamics of this system are similar to (1.2),(1.3) and (1.4). Although they are not exactly the same because one needs to include the influence of the cosmological constant in the equations. The complete set of equations (including the metric) is

$$ds^2 = \frac{l^2}{\cos^2 x} (-Ae^{-2\delta} dt^2 + A^{-1} dx^2 + \sin^2 x d\Omega^2), \quad (1.13)$$

$$\dot{\Phi} = (Ae^{-\delta}\Pi)' \quad \dot{\Pi} = \frac{1}{\tan^2 x} (\tan^2 x Ae^{-\delta}\Phi)', \quad (1.14)$$

$$A' = \frac{1 + 2\sin^2 x}{\sin x \cos x} (1 - A) - \sin x \cos x A (\Phi^2 + \Pi^2), \quad (1.15)$$

$$\delta' = -\sin x \cos x (\Phi^2 + \Pi^2). \quad (1.16)$$

In this system of equations A , δ , Φ and Π are functions of x , a generic dimensionless space-like coordinate related to the radial position that spans from 0 to $\pi/2$, and t , a dimensionless time-like coordinate. While the A and δ are functions related to the metric, Φ and Π are auxiliary functions related to the components of the Energy-momentum tensor. Their inter-dependence is obtained from the Einstein and Klein-Gordon equations, this inter-dependency will be demonstrated further in this document. From the Einstein equation, one can obtain another equation, the momentum constraint, given by

$$\dot{A} + 2 \sin x \cos x A^2 e^{-\delta} \Phi \Pi = 0. \quad (1.17)$$

This conservation equation was used to check the accuracy of the code. The initial data used in [5] is of the form

$$\Phi(0, x) = 0, \quad \Pi(0, x) = \frac{2\varepsilon}{\pi} e^{-\frac{4 \tan^2 x}{\pi^2 \sigma^2}}, \quad (1.18)$$

where σ is the field's width and ε is the field's amplitude.

While Choptuik [9] studied the phenomenon for several initial data families, in [5] only one family of initial data was used to study the collapse phenomenon. Bizoń et al. [5] concluded that, for a large amplitude, the wave packet collapses quickly at $r = 0$. We can see these evidences of this from the formation of an apparent horizon where the function A drops to zero. However, Bizoń et al. did not obtain a single critical point for the power law of the black hole mass as a function of the initial amplitude of the scalar field. They obtained several critical points, as we can see in Fig. 1.1. For all the critical values, Bizoń et al. concluded that, at the right of each critical point, the power law is the same that Choptuik obtained, with $\gamma \simeq 0.37$. In order to follow the collapse phenomenon, Bizoń et al. monitored the curvature scalar at the origin and concluded that $\varepsilon^{-2} \Pi^2(\varepsilon^2 t)$ gives, approximately, the same curve, independent of the field's intensity, ε . Additionally, arbitrary small fields start growing eventually. After

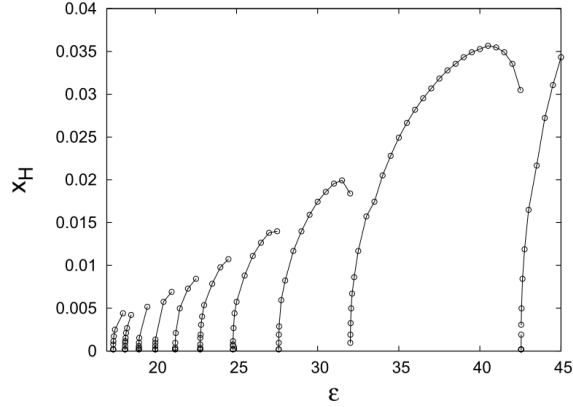


Figure 1.1: Horizon radius as a function of the amplitude of the initial data. The number of reflections off the AdS boundary before collapse varies from zero to nine (from right to left). Image taken from Ref. [5]. Note that the field's intensity is shown with a different convention, $4\pi G = 1$.

analysing the general dynamics of the scalar field in AdS, Bizoń et al. tried to apply weakly nonlinear perturbation theory. Although it was possible to obtain the early evolution of the system, they were not able to explain the process that caused the collapse.

In the same year, Jałmużna, Rostworowski and Bizoń [17] published a paper stating that the perturbative behaviour present in 3+1 dimensions is present in all $d > 3$ dimensions. This paper came as a refutation to an earlier paper from Garfinkle and Zayas [13]. The latter claimed that no black hole formation was observed for small values of the initial amplitude and, in such cases, the field would propagate indefinitely back and forth through the spacetime nearly following null geodesics.

Later, in 2012, Maliborski studied a timelike worldtube with a perfectly reflecting wall [20]. The initial analysis done by the author is the same as the one discussed in [5]. However, in this paper, the author studied the energy transfer into higher modes using Sobolev-type weighted energy norm. He concluded that the mirror did not influence the mode energy transfer, but allowed the reflection towards the center, where the pulse is focused repeatedly. Maliborski's article [20] was also useful to answer a question posed by Bizoń's and Rostworowski [5] regarding the influence of the cosmological constant in the system dynamics. Maliborski's work answers this question. Due to the nature of the systems with and without a cosmological constant, the sole purpose of a cosmological constant in such models is to make a spatial boundary. This boundary, like a mirror, repeatedly reflects the field back to the center, where the focusing phenomenon occurs.

In 2012, Buchel, Liebling and Lehner studied the formation of boson stars in AdS [7]. The authors successfully constructed linearly stable boson stars in AdS and their dynamics suggest that boson stars are also non-linearly stable. They studied the dependency of the apparent horizon location with the global charge and concluded that the two quantities are independent. Furthermore, they concluded that the linear dynamics of the field is also independent of the global charge. They also performed a spectral analysis of the field's evolution revealing an exponential growth in the spectral bandwidth. This behaviour is consistent with the evolution of the Π^2 function at the origin.

In 2013, Buchel, Lehner and Liebling [6] confirmed the collapse and black hole formation in AdS for

any scalar field's initial amplitude. Using the same metric as in [17] and, just as was done in [3], they studied the same problem with a complex scalar field. Using the rescaled quantities

$$\phi \rightarrow \frac{\phi}{\cos^{D-1} x}, \quad (1.19)$$

$$\Pi \rightarrow \frac{\Pi}{\cos^{D-1} x}, \quad (1.20)$$

$$\Phi \rightarrow \frac{\Phi}{\cos^{D-2} x}, \quad (1.21)$$

we can obtain the evolution equations

$$\dot{\Phi} = (Ae^{-\delta}\Pi)', \quad (1.22)$$

$$\dot{\Phi} = \frac{1}{\cos^{d-2} x} (\cos^{d-1} x Ae^{-\delta}\Pi)', \quad (1.23)$$

$$\dot{\Pi} = \frac{1}{\sin^{d-1} x} \left(\frac{\sin^{d-1} x}{\cos x} Ae^{-\delta}\Phi \right)'. \quad (1.24)$$

The profiles for the functions A and δ are obtained from the solution for the two spatial differential equations

$$A' = \frac{d-2+2\sin^2 x}{\sin x \cos x} (1-A) - \sin x \cos^{2d-1} x A \left(\frac{\Phi^2}{\cos^2 x} + \Pi^2 \right), \quad (1.25)$$

$$\delta' = -\sin x \cos^{2d-1} x \left(\frac{\Phi^2}{\cos^2 x} + \Pi^2 \right), \quad (1.26)$$

and we can check the accuracy of the code by monitoring the constraint equation

$$\dot{A} + 2 \sin x \cos^{2d-2} A^2 e^{-\delta} \Phi \Pi = 0. \quad (1.27)$$

For these equations there are two variables, x and t , that span from $x = 0$ to $x = \pi/2$ and from $t = t_i \doteq 0$ to $t \rightarrow +\infty$. Just like the other systems described in the present document, this system also needs to be well behaved at the boundaries. Taking this into consideration, the system behaves at the origin according to

$$\phi(t, x) = \phi_0(t) + \mathcal{O}(x^2), \quad (1.28)$$

$$A(t, x) = 1 + \mathcal{O}(x^2), \quad (1.29)$$

$$\delta(t, x) = \delta_0(t) + \mathcal{O}(x^2), \quad (1.30)$$

and, at spatial infinity, where we introduce the variable $\rho = \pi/2 - x$, the system behaves as

$$\phi(t, \rho) = \phi'_\infty(t)\rho + \mathcal{O}(\rho^3), \quad (1.31)$$

$$A(t, \rho) = 1 - M \frac{\sin^d \rho}{\cos^{d-2} \rho} + \mathcal{O}(\rho^{2d}), \quad (1.32)$$

$$\delta(t, \rho) = 0 + \mathcal{O}(\rho^{2d}). \quad (1.33)$$

In [6], the authors also analysed the spatial profile of the energy/mass density. The symmetry group for the complex scalar field is the $U(1)$ group. Therefore we can define a conserved quantity, a charge. This charge, along with the system's energy, can be tuned in the initial conditions. The equations are solved numerically using a finite-difference approximation in method-of-lines approach for the spatial differential equations and a third order accurate Runge-Kutta (RK3) time evolution scheme. An adaptive mesh refinement was used to add resolution where needed.

The authors of [6] performed some tests on their code and concluded that the solution converges, at least, as fast as third order. They also confirmed that the momentum constraint equation error decreases as the grid resolution increases. It was also verified that this result is also verified by the system's mass and charge error and that the resolution does not influence the collapse time of the scalar field. The authors of [6] found an instability towards higher frequencies in a finite size domain with reflective boundary conditions before spatial infinity in an asymptotic AdS. This was not initially expected because the field had no knowledge of the asymptotic nature of the spacetime, which suggested that the instability is a property of the bounded domain and not of the AdS. In [6], the authors concluded that the apparent horizon formation is rather insensitive to the field's global charge, in disagreement with previous literature [7]. In [6], the authors justify their results arguing that a perturbative analysis of the system is independent of the global charge. However, they realized that this argument is valid for the linear regime but may fail for the late-time evolution regime.

The authors of [6] studied the scalar field dependence on the σ parameter, the standard deviation of the initial field's profile, and concluded that when its value is larger than 0.4 the unstable growth seems to disappear, although they recognize that this result is not coherent with the semilinear wave equation in AdS. Although they claim to have found a stability region, they were unable to establish its domain, both in the amplitude spectrum and the spectral profile of the initial data. The thermalization region is therefore unknown for complex fields. This means the implications of these results for conformal field theories due to the irregular thermalization process for scalar fields with high dispersion in AdS remain as an open question.

More recently, in 2014, Balasubramanian et al. [4] also studied the linear stability of the real massless scalar field collapse and identify some similarities between the scalar field's behaviour and the dynamic evolution of a set of systems used to refer to the Fermi-Pasta-Ulam-Tsingou problem [11].

In the same year, Okawa et al. [24] studied the evolution of a real massive scalar field in a confined flat spacetime. They extended the results for scalar fields giving special attention to lower intensity. In their study there were more than one thousand reflections and they verified that the tendency of the massive field is to collapse and form a black hole, with the exception of some islands of stability through the range of the field's amplitude. It is also important to note that a field with small amplitude may collapse after thousands of reflection even if it is outside the range of the simulation time and, because of this, it is mandatory to find a deeper analytical understanding of the phenomena present in this set of systems.

1.3 Original Contributions

This work focuses on studying the stability of the AdS spacetime. The ADM formalism was used to derive the differential equations from the Einstein and the Klein-Gordon equation. The code was fully developed by the author and the co-supervisor. The simulations are run in 3 machines, the author's personal, in a particular server and in CENTRA's cluster "Baltasar Seven-Suns". The time to run a simulation until reaching collapse varies from thirty minutes to four days per reflection. For each simulation, the apparent horizon and the collapse time were observed and recorded. The evolution of the curvature at the origin was also monitored for long time runs in order to establish its behaviour.

1.4 Structure of the Thesis

The remainder of this document is structured as follows: in Chapter 2, an introduction to the AdS spacetime is presented along with the extensions necessary to incorporate scalar fields. In Chapter 3 the numerical results are briefly discussed along with the numerical methods developed. Chapter 4 lays the main conclusions of this study and suggests some ideas for future research.

Chapter 2

Theory

In this chapter we will start with a dynamical analysis of a massless scalar field using the Klein-Gordon equation in an AdS spacetime using the ADM formalism in section 2.2. In section 2.2.1 we derived a system of differential equations that rule the dynamics of the massless scalar field in AdS.

2.1 Overview of the AdS spacetime

In this section, we will introduce and describe the properties of the AdS space and deduce the system we are going to use to analyse the evolution of scalar fields in AdS [21].

The AdS_{d+1} space is a maximally symmetric solution of the Einstein equation for an empty Universe with a negative cosmological constant. It can be defined as the pseudo-spherical or hyperboloid hypersurface as

$$-(X^0)^2 + \sum_{k=1}^d (X^k)^2 - (X^{d+1})^2 = -l^2, \quad (2.1)$$

embedded in a flat \mathbb{R}^{d+2} with an $O(d,2)$ symmetry. In this space we use the line element

$$ds^2 = -(dX^0)^2 + \sum_{k=1}^d (dX^k)^2 - (dX^{d+1})^2. \quad (2.2)$$

We are able to use a coordinate transformation

$$\begin{cases} X^0 = l \sec x \cos t \\ X^{d+1} = l \sec x \sin t \\ X^i = l \tan x n^i \quad 1 < i \leq d \end{cases}, \quad \sum_{i=1}^d (n^i)^2 = 1 \quad (2.3)$$

to work out the line element and obtain, using $d = 3$ for our system,

$$\begin{aligned}
ds^2 &= - \left(\frac{\partial X^0}{\partial x} \right)^2 dx^2 - \left(\frac{\partial X^0}{\partial t} \right)^2 dt^2 + \sum_{k=1}^d \left(\frac{dX^k}{dx} \right)^2 dx^2 \\
&\quad + \sum_{k=1}^d \left(\frac{dX^k}{dn^i} \right)^2 dn^i{}^2 - \left(\frac{\partial X^4}{\partial x} \right)^2 dx^2 - \left(\frac{\partial X^4}{\partial t} \right)^2 dt^2 \Leftrightarrow \\
\Leftrightarrow ds^2 &= - \left(l \cos t \frac{\sin x}{\cos^2 x} \right)^2 dx^2 - \left(l \frac{\sin t}{\cos x} \right)^2 dt^2 + \left(\frac{1}{\cos^2 x} dx^2 + \tan^2 x d\Omega_{d-1}^2 \right) \\
&\quad - \left(l \sin t \frac{\sin x}{\cos^2 x} \right)^2 dx^2 - \left(l \frac{\cos t}{\cos x} \right)^2 dt^2 \Leftrightarrow \\
\Leftrightarrow ds^2 &= \frac{l^2}{\cos^2 x} \left(-dt^2 - \left(\tan^2 x - \frac{1}{\cos^2 x} \right) dx^2 + \sin^2 x d\Omega_{d-1}^2 \right) \Leftrightarrow \\
\Leftrightarrow ds^2 &= \frac{l^2}{\cos^2 x} (-dt^2 + dx^2 + \sin^2 x d\Omega_{d-1}^2). \tag{2.4}
\end{aligned}$$

In the previous derivation, we can identify $r = l \tan x$ as the radial coordinate transformation. We can identify the conformal spacial infinity at $x = \pi/2$ and the bulk of the AdS spacetime as a timelike cylinder centered at $x = 0$ and with radius $x = \pi/2$. This line element represents the solution of the Einstein equation, $G_{ab} + \Lambda g_{ab} = 0$, of the empty Universe with a negative cosmological constant, $\Lambda = -d(d-1)/(2l^2)$. Our Universe is not an empty one and, as such, we can not use this line element, but we can use it to motivate a general line element for the system we are going to study. Our field will be a spherically symmetric field and we can use this symmetry to provide our line element the degrees of freedom necessary to satisfy the Einstein equation in the presence of such field.

In our model we will use the metric ansatz

$$ds^2 = \frac{l^2}{\cos^2 x} (-Ae^{-2\delta} dt^2 + A^{-1} dx^2 + \sin^2 x d\Omega_{d-1}^2). \tag{2.5}$$

In this ansatz, the angular components of the metric remain unmodified by the additional degrees of freedom. Furthermore, the A function is motivated by the field's collapse while the δ function is introduced in such way that it will directly influence the Courant stability condition later when we attempt to solve this system numerically.

2.2 Dynamic model of the AdS spacetime

In this section, we will start from the Einstein equation and the Klein-Gordon equation

$$G_{ab} + \Lambda g_{ab} = 8\pi T_{ab} = 8\pi (\partial_a \phi \partial_b \phi - \frac{1}{2} g_{ab} (\partial \phi)^2), \tag{2.6}$$

$$g^{ab} \nabla_a \nabla_b \phi = 0, \tag{2.7}$$

and, using the metric ansatz in [5],

$$g_{ab} = \frac{l^2}{\cos^2 x} \text{diag}(-Ae^{-2\delta}, A^{-1}, \sin^2 x, \sin^2 x \sin^2 \theta), \quad (2.8)$$

deduce the evolution equation of the system. In the Einstein equation, eq. 2.6, the cosmological constant Λ is related with the length scale as $l^2 = -3/\Lambda$.

Before deducing the evolution equations, we introduce the ADM formalism. This formalism is usually useful when dealing with numerical problems in general relativity.

The ADM formalism was introduced in 1959 by Richard Arnowitt, Stanley Deser and Charles Misner [2]. For this formalism, we slice the spacetime into spacelike leaves and project the quantities in the equations we are working on into their space and time components. For a detail overview of the ADM formalism, without the cosmological constant, see [14]. Before working out the Einstein equation, one begins by defining the lapse function, N , the shift vector, N_i , and the induced metric, γ_{ij} , from the four-dimensional general metric, ${}^4g_{\mu\nu}$, as

$$N \equiv \sqrt{g_{00}} = \frac{l}{\cos x} \sqrt{Ae^{-\delta}}, \quad (2.9)$$

$$N_i \equiv g_{0i} = (0, 0, 0), \quad (2.10)$$

$$\gamma_{ij} \equiv g_{ij} = \frac{l^2}{\cos^2 x} \text{diag}(A^{-1}, \sin^2 x, \sin^2 x \sin^2 \theta). \quad (2.11)$$

and the extrinsic curvature as

$$K_{ij} = -\frac{1}{2} \frac{\partial \gamma_{ij}}{\partial t} = \text{diag}\left(-\frac{1}{2} \frac{\dot{A}}{A^2}, 0, 0\right), \quad (2.12)$$

where the indexes i and j are associated with the spatial components via the ADM formalism and they range from one to three while the indexes μ and ν are associated with the standard tensorial formalism and they range from zero to three. It is very important to understand the appropriate rules of tensorial manipulation while working out these quantities because some equalities are not trivially obtained, such as $\gamma^{ij} = g^{ij}$. This previous expression is, in general, incorrect because the induced metric has a dependence on the shift vector components.

As one can observe from the previous definitions, the ADM formalism takes the general metric g_{ab} and projects it into its time-time, space-time and space-space components. By doing the same thing to the Einstein equation the dynamic equations for the system described in [5] can be obtained.

2.2.1 Projections of the Einstein equation

Projecting the Einstein equation twice along the time unit vector results in

$${}^4R_{ab}n^a n^b - \frac{1}{2} {}^4R + \Lambda = 8\pi T_{ab}n^a n^b. \quad (2.13)$$

This result can be combined with the scalar Gauss equation

$${}^4R + 2{}^4R_{ab}n^an^b = R + K^2 - K_{ij}K^{ij} \quad (2.14)$$

to obtain the Hamiltonian constraint

$$R + K^2 - K_{ij}K^{ij} - 2\Lambda = 16\pi E, \quad (2.15)$$

given that E is the time-time projection of the Energy-Momentum Tensor in the Einstein Equation. The vacuum solution is obtained by taking $E \rightarrow 0$, $A \rightarrow 1$, this second condition means that $K_{ij} \rightarrow 0$. In this case we obtain $R = 2\Lambda = -6/l^2$. One can also project the Einstein equation once along the unit timelike vector, resulting in a vectorial entity, and once along the hyper-surface orthogonal to the time unit vector thus obtaining a vectorial spatial projection. In this case, the momentum constraint is obtained,

$$D_j K^j_i - D_i K = 8\pi p_i, \quad (2.16)$$

where $D_i = \gamma_i^j \partial_j$ is the spatial projection of the tensorial partial derivative and p_i is the space-time projection of the Energy-Momentum Tensor.

Finally, we project the Einstein equation twice spatially and we obtain the evolution equation

$$\begin{aligned} \mathcal{L}_n K_{ab} &= -8\pi N \left(S_{ab} - \frac{1}{2}(S - E)\gamma_{ab} \right) - N\Lambda\gamma_{ab} - D_a D_b N + NR_{ab} + NK K_{ab} - 2NK_{al}K_b^l \\ &= -8\pi N \left(S_{ab} - \frac{1}{2}(S - E)\gamma_{ab} \right) - N\Lambda\gamma_{ab} - \partial_a \partial_b N + \Gamma_{ab}^l \partial_l N + NR_{ab} + NK K_{ab} - 2NK_{al}K_b^l. \end{aligned} \quad (2.17)$$

where \mathcal{L}_n is the Lie derivative along the vector \vec{n} and S_{ab} is the space-space projection of the Energy-Momentum Tensor. If we use the ADM formalism, the Lie derivative along \vec{n} is

$$\mathcal{L}_n = \frac{1}{N} \frac{\partial}{\partial t}. \quad (2.18)$$

With these equations we are able to obtain the system's equations for the profiles of the geometric functions.

2.2.2 The evolution equations

From the equation described above one can obtain the dynamic equations described in [5].

One can deduce what we will obtain on the left-hand side on the projections of the Einstein equation and, therefore, to the geometric nature of the evolution equation. Using the functions $\Phi = \phi'$ and $\Pi = A^{-1}e^\delta \dot{\phi}$, we are able to simplify the expression for the evolution of the scalar field. These equations

have terms concerning the energy, momentum and stress tensors. The non-zero tensors take the form

$$E = \frac{1}{2} \frac{A^2}{N^2} e^{-2\delta} (\Pi^2 + \Phi^2) = \frac{1}{2} \frac{A \cos^2 x}{l^2} (\Pi^2 + \Phi^2), \quad (2.19)$$

$$P_x = T_{10} = \frac{1}{N} (\partial_x \phi)^2 (\partial_t \phi)^2 = -\frac{\sqrt{A} \cos x}{l} \Pi \Phi, \quad (2.20)$$

$$S_{rr} = (\partial_r \phi)^2 - \gamma_{(rr)} g^{ab} \partial_a \phi \partial_b \phi = \frac{1}{2} (\Phi^2 + \Pi^2), \quad (2.21)$$

$$S_{\theta\theta} = \frac{1}{2} A \sin^2 x (\Pi^2 - \Phi^2), \quad (2.22)$$

$$S_{\varphi\varphi} = \frac{1}{2} A \sin^2 x \sin^2 \theta (\Pi^2 - \Phi^2). \quad (2.23)$$

In these equations we use the variable transformations $\Phi = \phi'$ and $\Pi = A^{-1} e^{\delta} \dot{\phi}$, where the prime and the over-dot stand for the x and t derivative, respectively. By applying the identities (2.19) to (2.23) to the constraint equation present previously, eq. (2.15) and eq. (2.16), we obtain the differential equation for the profiles of the A and δ functions. The Hamiltonian and momentum constraint equations result in, respectively,

$$A'(t, x) = \frac{1 + 2 \sin^2 x}{\sin x \cos x} (1 - A) - 4\pi \sin x \cos x A (\Phi^2 + \Pi^2), \quad (2.24)$$

$$\dot{A}(t, x) = -4\pi \sin x \cos x A^2 \Pi \Phi. \quad (2.25)$$

Note that the ADM formalism states that these constraint only need to be verified for the initial data. These constraints are a result of the Bianchi identities[23].

The evolution equations give us a set of nine of equations, six of which are trivial, because they use different indexes and the off-diagonal equations use off-diagonal terms of the induced metric, and the other three identical equations that result in the linear combination of the equations (2.24) and

$$\delta' = -4\pi \sin x \cos x (\Phi^2 + \Pi^2). \quad (2.26)$$

Because of this, the profile equation for A must be solved at all times through the evolution of the system.

At this point we are able to find the solutions of A and δ functions for a set of data, but it is necessary to evolve it through time. From these definitions one can trivially obtain the equation

$$\dot{\Phi} = (A e^{-\delta} \Pi)', \quad (2.27)$$

and, combining these definitions with the Klein-Gordon equation, one can obtain

$$g^{ab} \nabla_a \nabla_b \phi = 0 \Leftrightarrow \dot{\Pi} = \frac{1}{\tan^2 x} (\tan^2 x A e^{-\delta} \Phi)'. \quad (2.28)$$

To sum it up, we derived the complete system of equations that rule the evolution of a massless

spherically symmetric scalar field,

$$\begin{cases} \dot{\Phi} = (Ae^{-\delta}\Pi)' \\ \dot{\Pi} = \frac{(\tan^2 x Ae^{-\delta}\Pi)'}{\tan^2 x} \\ A' = \frac{1+2\sin^2 x}{\sin x \cos x}(1-A) - 4\pi \sin x \cos x A (\Phi^2 + \Pi^2) \\ \delta' = 4\pi \sin x \cos x (\Phi^2 + \Pi^2), \end{cases} \quad (2.29)$$

where Φ , Π , A and δ are all functions of t and x where $t \in]0, +\infty[$ and $x \in]0, \pi/2[$. We do not know if this system has an analytical solution and, because of this, we will need to use numerical methods to find a solution for it.

As for the boundary conditions, we assume that the physically meaningful functions are smooth and that we place an observer at the origin. This means that,

$$\phi(t, x) = \phi_0(t) + \mathcal{O}(x^2), \quad (2.30)$$

$$A(t, x) = 1 + \mathcal{O}(x^2), \quad (2.31)$$

$$\delta(t, x) = \mathcal{O}(x^2). \quad (2.32)$$

The asymptotic behaviour of ϕ represents the matter background density, which does not influence the evolution equations.

In the three dimensional case the asymptotic behaviour at spatial infinity is

$$\phi(t, x) = f_\infty(t)\rho^3 + \mathcal{O}(\rho^5), \quad (2.33)$$

$$A(t, x) = 1 - M\rho^3 + \mathcal{O}(\rho^5), \quad (2.34)$$

$$\delta(t, x) = \delta_\infty(t) + \mathcal{O}(\rho^6), \quad (2.35)$$

where $\rho = \pi/2 - x$, δ_∞ and f_∞ are free functions obtained from the power series expansion at spatial infinity and M is the system's total mass/energy.

This concludes the theoretical overview of the literature and the system we are studying. In the next chapter we will discuss the numerical results obtained so far.

Chapter 3

Numerical Methods and Results

In this chapter, we discuss the approach followed to solve the dynamic equations described in the final section of the previous chapter. We begin by solving the differential equations to obtain the initial profiles of the A and δ functions, presented in section 3.1, along with convergence tests and integrate in these solutions the time-evolution of the Φ and Π functions.

The equations that need to be solved are non-linear and, in general, have no analytical solution. In such case the appropriate approach is to find approximate solutions using numerical techniques.

3.1 Spatial profiles and Convergence tests

Before computing the time evolution of the system as a whole, we study the differential equations that allow us to obtain the initial spatial profiles of the geometric functions A and δ . For every simulation to compute the solution for the spatial profiles of the A and δ functions and for the time evolution of the system Gaussian initial matter profiles will be used

$$\Phi(0, x) = 0, \quad (3.1)$$

$$\Pi(0, x) = \frac{2\varepsilon}{\pi} e^{-\frac{4 \tan^2 x}{\pi^2 \sigma^2}}. \quad (3.2)$$

The first attempt to solve this system follows the same approach as that described in [23], which is to discretize and solve an one dimensional Poisson equation with a source term using the Jacobi method or the successive over-relaxation (SOR) method. Using the Poisson-like equation with a mass-like term is motivated by the Newtonian limit of GR. Recalling eq. (2.24),

$$A'(t, x) = \frac{1 + 2 \sin^2 x}{\sin x \cos x} (1 - A) - 4\pi \sin x \cos x A (\Phi^2 + \Pi^2).$$

The right hand side represents the source term of the Poisson equation. A source term of this form is not well-behaved at the origin, and the discretization gives rise to large numerical errors around this region. This affects the whole behaviour of the function because, in this system, the boundary conditions are set at the origin and any error near the origin will be propagated and amplified throughout the spatial

grid. Therefore, any numerical error will propagate through the entire grid, due to the dependence of each value of one particular grid point with its neighbour points.

Eq. (2.24) is a first order differential equation. To apply a second order Jacobi method one needs a second order differential equation. If we differentiate eq. (2.24) with respect to x , we obtain a second order differential equation,

$$\begin{aligned}
 A''(t, x) = & (-\csc^2 x + 2\sec^2 x)(1 - A) - \\
 & - (\cot x + 2\tan x + \cos x \sin x (\Pi(t, x)^2 + \Phi(t, x)^2)) A'(t, x) \\
 & - A(t, x) (\cos 2x (\Pi(t, x)^2 + \Phi(t, x)^2) + \sin 2x (\Pi(t, x)\Pi'(t, x) + \Phi(t, x)\Phi'(t, x))). \quad (3.3)
 \end{aligned}$$

We cannot impose a boundary condition at $x = 0$ due to the indetermination of the right hand side of eq. (2.24). We can, however set its value at the point closest to the origin, $\Delta x = \pi/(2N)$, where N is the number of grid points. The simplest approach is to force the A function, at dx , to be $A(t, dx) = 1$. Using the same approach, one can define the spatial derivative of the $A(t, x)$ function near the origin as $A'(t, dx) = 0$, which can be used for the second order differential equation regarding the same function. Before going into a fully numerical approach, the two differential equations were solved using the Mathematica software [28] in order to get some insight on what the solution is suppose to look like. The solution of the two differential equation to obtain the A function for the initial data profile simulating $N = 2000$ and $\varepsilon = 10$ is plotted in fig. 3.1. We realized later that we should consider the Taylor expansion at the origin and use it for the boundary condition. The Taylor series, which was not used initially, of the A and δ functions are

$$A(t, dx) = 1 - \frac{4\pi}{3}\Pi^2(t, 0)dx^2, \quad (3.4)$$

$$\delta(t, dx) = 2\pi\Pi^2(t, 0)dx^2. \quad (3.5)$$

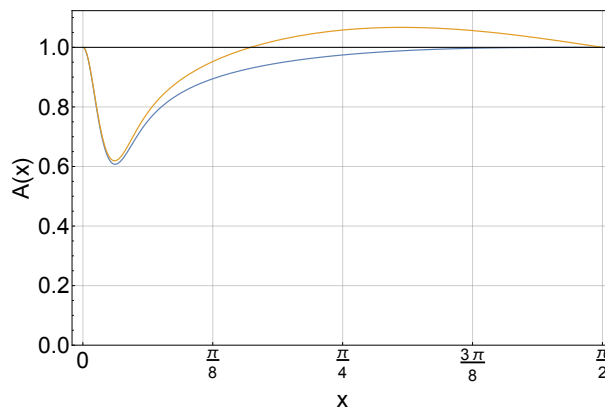


Figure 3.1: Representation of A as a function of x , with fixed $\varepsilon = 10$. The boundary conditions are $A(0, \pi/4000) = 1$ and, for the second order equation, $A'(0, \pi/4000) = 0$ to simulate $N = 2000$. A Mathematica's internal algorithm was used to solve the first order differential equation (blue line) and the second order differential equation (yellow line).

The solution using second order method, presented in fig. 3.1, was discarded because the results suggest that it does not give accurate solutions.

After this failed attempt using a second order method, we tried to implement a straight forward finite difference method. The finite differences expressions for the first derivative up to first, second and fourth order, using constant grid discretization dx and the backward scheme, are

$$f^{(1)}(x) = \frac{-f(x-dx) + f(x)}{dx} + \mathcal{O}(dx), \quad (3.6)$$

$$f^{(1)}(x) = \frac{f(x-2dx) - 4f(x-dx) + 3f(x)}{2dx} + \mathcal{O}(dx^2), \quad (3.7)$$

$$f^{(1)}(x) = \frac{25f(x-4dx) - 48f(x-3dx) + 36f(x-2dx) - 16f(x-dx) + 3f(x)}{12dx} + \mathcal{O}(dx^4). \quad (3.8)$$

We used a backward first order scheme to obtain a profile solution for the A function. We compared the numerical solution obtained using our algorithm with the first order solution obtained using Mathematica's default method. We verified that our numerical solution matches Mathematica's first order solution. Although this represents a step in the right direction, it is not enough to validate our solution. In order to verify our results we performed a convergence test for the numerical solutions. We computed a ratio between the numerical solutions obtained for different amounts of grid points, N , at a particular position x ,

$$r_N = \frac{f_{N_1} - f_{N_2}}{f_{N_2} - f_{N_3}}, \quad (3.9)$$

where we define N_1 and use $N_2 = N_1 + M_1$ and $N_3 = N_1 + M_2$, where M_1 and M_2 are two constants with different values. In our tests, we used $M_1 = 500$ and $M_2 = 1000$. We can obtain the expected ratio with the discretization used because

$$f_A(x) = f_{N_1}(x) + \mathcal{O}(dx^n) \quad (3.10)$$

where f_A is the analytical solution and n is the method's order. We can obtain a theoretical value for r

$$r_t = \frac{dx_{N_1}^n - dx_{N_2}^n}{dx_{N_3}^n - dx_{N_2}^n} \quad (3.11)$$

The r ratio is defined so that it depends on the method's consistency but not on the details of the differential equation to be solved. In order to simplify the analysis we computed the ratio $R = r_N/r_t$, which should go asymptotically to 1 as N goes to infinity. This means that the numerical solutions will converge to the continuum limit solution. Our results show that the A function converges as the R ratio goes asymptotically to unity. For the first order method we obtained Fig. 3.2.

After testing the results for the first order scheme, we computed the solution for the same equation using a backward second order scheme and a backward fourth order scheme. While computing the second order scheme, we also tried to solve it with an implicit centered second order scheme, but it proved to be too slow and it provided worse results than the previously obtained with an explicit method.

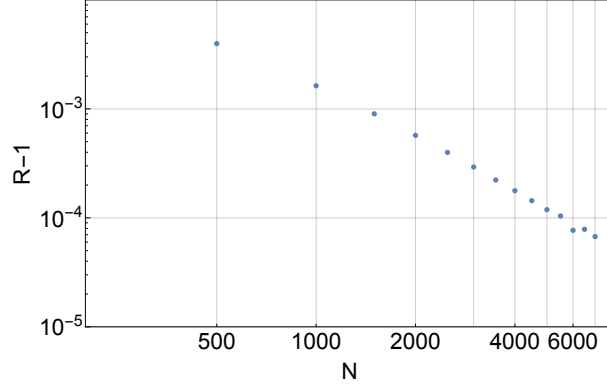


Figure 3.2: First order ($R - 1$) as a function of the number of grid points, N . Both axes are logarithmic scaled.

Before proceeding to the analysis of eq. (2.26) one can draw some conclusions from the tests performed previously. One finds that it is not viable to use the second order equations due to error propagation from the origin. Using implicit methods is also not viable because it consumes a lot of time and, in this case, the results are not as good as the ones obtained with an explicit method.

We identified two possible ways to implement the boundary conditions. One can use the symmetry of the functions near the origin to determine the first n grid points, or we can use the asymptotic behaviour of the function to determine its Taylor series and implement the first n points, where n is the method's order. If the symmetry of the function is used one must solve a system of n equations to find n variables, the first n grid points. If the asymptotic behaviour of the function is used one must derive the asymptotic behaviour of the function in order to determine the first n grid points. For the first and second order algorithms the symmetry approach is perfectly viable, however, as the method's order increases, so does the complexity of the solution for the grid points near the origin. This is so severe that one must use the asymptotic behaviour for fourth order methods.

In order to obtain the δ function profile using eq. (2.26),

$$\delta' = -4\pi \sin x \cos x (\Pi^2 + \Phi^2),$$

we followed the same approach used to solve the A function, the finite difference first derivative. For the higher order method, the point closest to the origin was set as $\delta(t, dx) = -2\pi \Pi^2(t, 0) dx^2$. This approach can then be extended to the next n points by using a n -th order method. The solution for the δ function using the initial data using $N = 1000$ and $\varepsilon = 10$ is presented in fig. 3.3.

This concludes the resolution of the spatial differential equations and respective tests to check the algorithm. We were able to obtain the A and δ functions profiles using the Π and Φ functions. In the next section we will study the time evolution of the system.

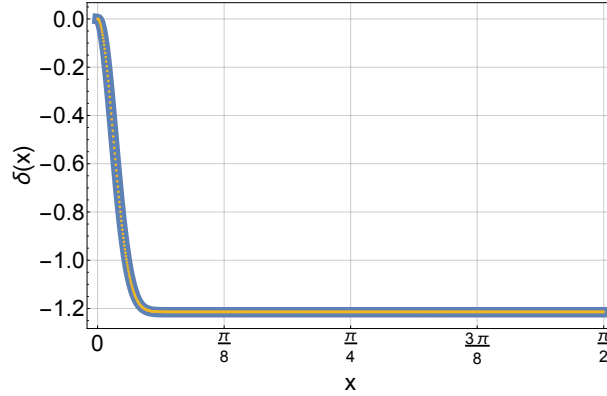


Figure 3.3: Representation of the δ function as a function of x using Mathematica's algorithm (blue line) and using a numerical algorithm (orange dots). The thickness of the blue line serves only as a visual aid as the two functions overlap almost perfectly.

3.2 Time evolution

In the previous section we solved numerically the differential equations (2.24) and (2.26) to obtain the geometric functions A and δ profile. After we computed the profiles for these functions we are able to evolve the Π and Φ functions. In order to do this we will use the differential equations

$$\begin{cases} \dot{\Phi}(t, x) = (Ae^{-\delta}\Pi)' \\ \dot{\Pi}(t, x) = \frac{(\tan^2 x Ae^{-\delta}\Pi)'}{\tan^2 x} \end{cases}, \quad (3.12)$$

using, as boundary condition at the origin,

$$\begin{cases} \Phi(t, x) = \mathcal{O}(x) \\ \Pi(t, x) = \Pi_0(t) + \mathcal{O}(x^2) \end{cases}, \quad (3.13)$$

and, as asymptotic behaviour at spatial infinity,

$$\begin{cases} \Phi(t, x) = \Phi_\infty'''(t)\rho^2 + \mathcal{O}(\rho^4) \\ \Pi(t, x) = \Pi_\infty''(t)\rho^3 + \mathcal{O}(\rho^5) \end{cases}. \quad (3.14)$$

Before we evolve the system through time, one must consider the Courant-Friedrichs-Lewy (CFL) condition. The CFL condition is a necessary condition that bounds the time-step value we can have in any system. We will not present a detailed demonstration of the CFL condition for this system. Although this does not represent a formal demonstration, we can qualitatively deduce that the CFL condition for this system, or the Klein-Gordon equation, is an adaptation of the CFL condition for the wave equation. We can use their similarities to understand the constraints we need to impose on our code in order to have a stable solution. The CFL condition for this system, using a fourth order spatial derivative and a

fourth order time evolution scheme, is

$$C_{max} \cong \frac{dt}{dx} \rightarrow e^{-\delta} \frac{\Delta t}{\Delta x}. \quad (3.15)$$

The δ function changes along the grid and we need all the grid points at the same time. The δ function decreases monotonically. This is a very useful property as it allows us to identify the minimum of the δ function, at spatial infinity, and replace its value in the CFL condition. Thus, the CFL condition will be

$$C_{max} \cong e^{-\delta(t,\pi/2)} \frac{\Delta t}{\Delta x}. \quad (3.16)$$

As this is not a formal derivation of the CFL condition, we will use this approach with a lower value of C , ideally between $1/6$ and $1/3$ [21]. In our code, in particular, we use $C = 1/4$. Note that this condition means that the time taken to perform one simulation grows quadratically with the grid resolution.

There are several known algorithms at our disposal in order to compute a time-evolving solution. Our first attempt consists in a straight forward Euler method with a first order spatial scheme. It was observed that the solution's error order is too high for us to obtain a reliable numerical solution.

These equations are non-linear and it is not trivial to verify the consistency of the methods only from the solutions obtained. Therefore we used the wave equation in order to test this scheme and concluded that a one-sided scheme does not allow the wave equation to propagate in one of the directions because one does not provide the method the information to do so. In this case, we obtain the transport equation [25].

After ruling out the first order approach, we tried to solve the system using an explicit backward scheme to compute the spatial profiles for the A and δ functions and a centered scheme to compute the spatial derivatives in the evolution equations. We were able to evolve the outgoing wave up until it reached the midpoint of the grid, where the numerical errors reached, approximately, the intensity of the wave. At this point we stopped the simulations because further letting the system evolve would only lead to larger errors in the solution, as one can see from the time evolution presented in fig. 3.4, plotting the Π and Φ with a factor of $\tan(x)$ in order to show a propagating wave with constant amplitude. One can clearly see that the numerical error starts to grow near the origin to a point where it becomes larger than the propagating wave between $t = 120 \times 10^{-3}$ and $t = 130 \times 10^{-3}$. For this simulation we used a constant $dt = 10^{-4}$ as, at the time, we were not aware of the constraint imposed by the CFL condition. This also serves to stress the need to consider the CFL condition in this particular numerical problem.

At that time, it was our belief that the errors were a consequence of the method's order. We improved the method to fourth order to obtain better results and to be able to let the field evolve for a longer period of time. We verified that the error growth through time of the fourth order method was similar to that of the second order method. From the evolution presented in fig. 3.5, one may verify that, although the error growth depends on the methods' order, it does not depend on the number of grid points for both orders. Furthermore, we managed to evolve the field for a full grid length before the errors became too large to identify the wave.

These errors rose to a magnitude comparable to the field's due to the $0/0$ indetermination of the right

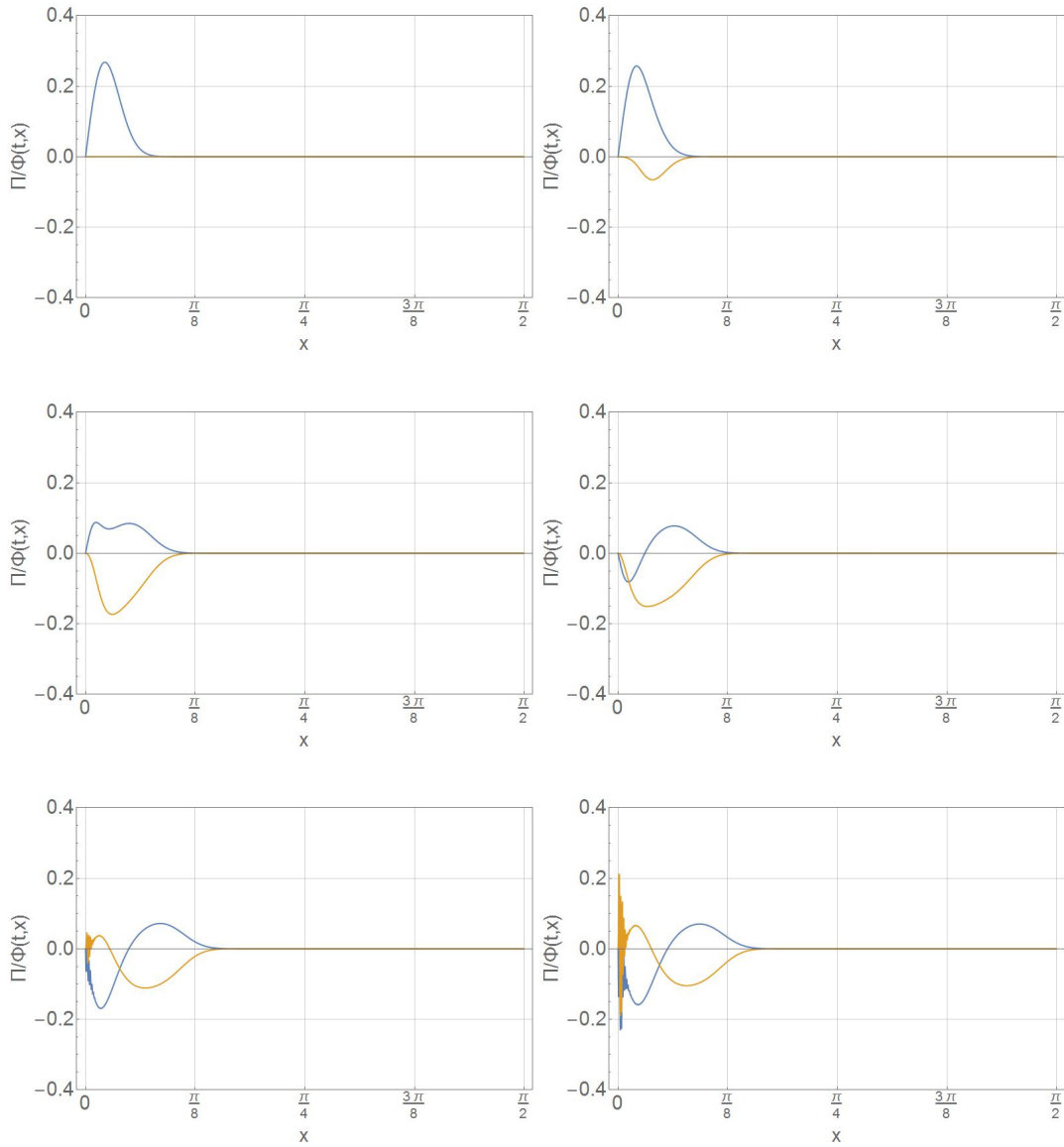


Figure 3.4: Profiles of $\tan(x)\Pi$, represented with a blue line, and $\tan(x)\Phi$ functions, represented with a orange line, with an initial intensity $\epsilon = 10$, at $t = 0$, $t = 10 \times 10^{-3}$, $t = 50 \times 10^{-3}$, $t = 80 \times 10^{-3}$, $t = 120 \times 10^{-3}$ and $t = 130 \times 10^{-3}$, timely ordered. For this time evolution, the algorithm used consisted in a straight forward second order finite difference method with a second order Runge Kutta method with $N = 1000$ and $\Delta t = 10^4$.

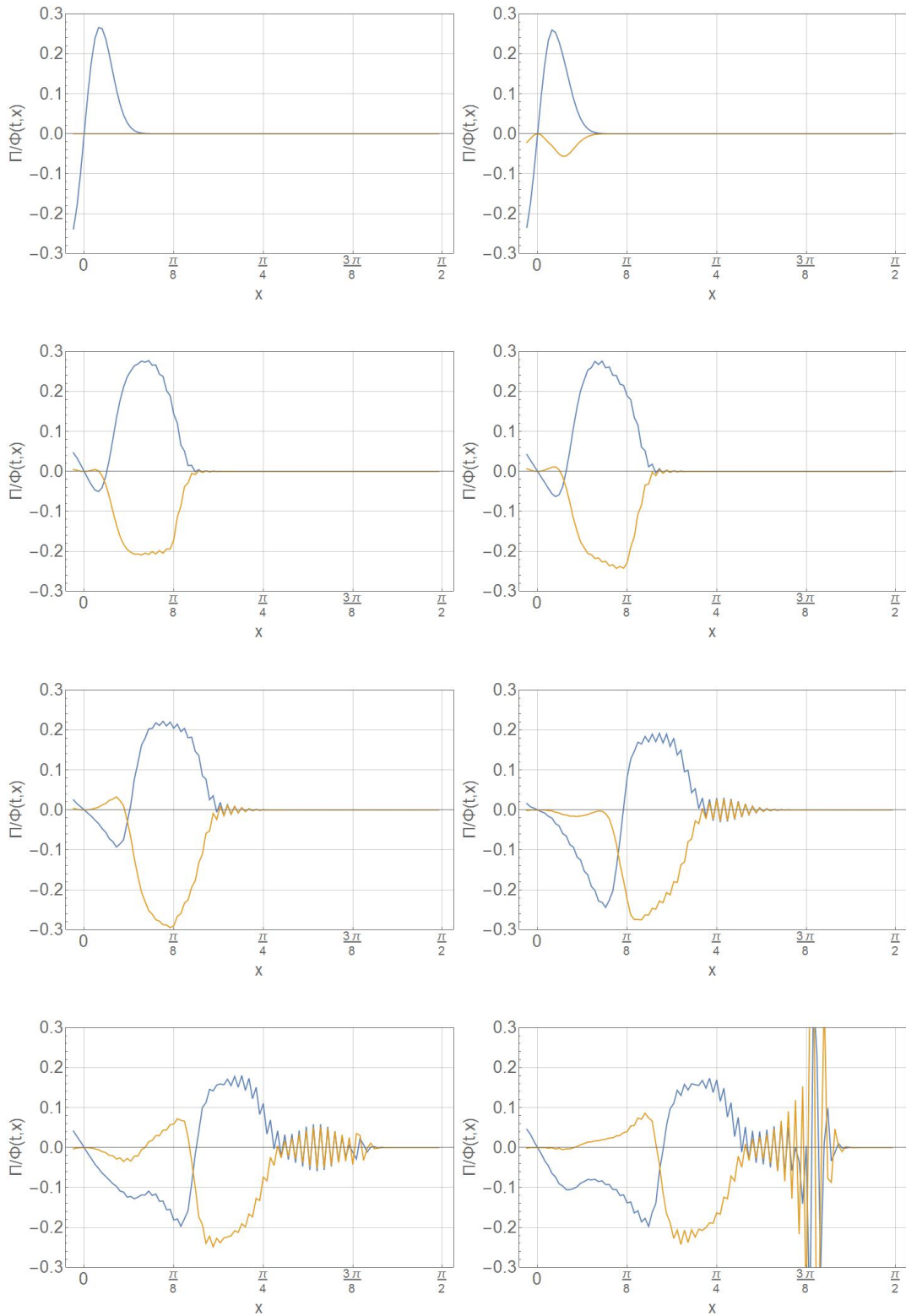


Figure 3.5: Profiles of $\tan(x)\Pi$, represented with a blue line, and $\tan(x)\Phi$ functions, represented with a orange line, with an initial intensity $\epsilon = 10$, at $t = 0$, $t = 10 \times 10^{-3}$, $t = 130 \times 10^{-3}$, $t = 150 \times 10^{-3}$, $t = 200 \times 10^{-3}$, $t = 300 \times 10^{-3}$, $t = 400 \times 10^{-3}$ and $t = 450 \times 10^{-3}$, timely ordered. In this case, the algorithm used consisted in a forward fourth order finite difference method with a fourth order Runge Kutta method with $N = 100$ and a variable dt , according to the CFL condition.

hand side of Π 's evolution equation at the origin, or ∞/∞ at spatial infinity [21]. In three dimensions, as is our case, we take Π 's evolution equation

$$\dot{\Pi} = (Ae^{-\delta}\Phi)' + 2\frac{Ae^{-\delta}\Phi}{\sin x \cos x}, \quad (3.17)$$

and use the expression [21]

$$\frac{Ae^{-\delta}\Phi}{\sin x \cos x} = \frac{(Ae^{-\delta}\Phi)'}{\cos 2x} - \frac{1}{2} \tan 2x \left(\frac{Ae^{-\delta}\Phi}{\sin x \cos x} \right)', \quad (3.18)$$

to make the indetermination vanish at the boundaries. Although this expression can be used for the entire grid, it gives us another indetermination at $x = \pi/4$. This is not problematic because we can choose to use this expression where the indeterminations are present. In order to do this, we divided our grid in four equal parts. In the extremes, between 0 and $\pi/8$ and between $3\pi/8$ and $\pi/2$, we apply the replacement expression in the center of the grid, between $\pi/8$ and $3\pi/8$, we do not apply the replacement expression because it would generate an unwanted indetermination where there is none.

Also, for computational purposes, we defined an auxiliary function $B = A - 1$. This does not have a major impact on the equations, as the boundary condition at the origin remains even. The equation to obtain the profile for the B function is

$$\dot{B} = -\frac{1 + 2\sin^2 x}{\sin x \cos x} B - 4\pi \sin x \cos x (B + 1) (\Phi^2 + \Pi^2). \quad (3.19)$$

This approach's advantage is that it makes the asymptotic behaviour at spatial infinity clearer as the Taylor series of the B function near spatial infinity is odd, $B = -2M\rho^3 - \mathcal{O}(\rho^6)$.

The discussion up to this point describes all the procedures and mathematical nuances one must consider while computing a numerical solution for this system. The code used to solve this system uses the fourth order Runge-Kutta method, which is the fourth order extension of the midpoint method, or second order Runge-Kutta method, and all the details we discussed in this section.

This concludes the study of the field's evolution. In the next section we will discuss the numerical results and conclude with their implications for the stability of the AdS spacetime.

3.3 The stability of the AdS spacetime

In this section we will discuss the results obtained from our simulations and compare them with the literature. We evolved the system until it collapsed using 16385 ($2^{14} + 1$) and 32769 ($2^{15} + 1$) grid points.

Theoretically, the field's collapse condition is $A(t, x) = 0$. Numerically, it is not possible to reach such condition. Our solution was to accept that the collapse position will have an error associated. The collapse condition used is $A(t, x) \leq C/N$, where the constant $C = 2^{16}/100$. This value has no particular meaning and it is slightly larger and less restrictive than the value proposed by Maliborski and Rostworowski [21]. This condition means that if, at any point in time, in some place, the A function went below the indicated threshold, the field collapsed and a black hole formed. While attempting to

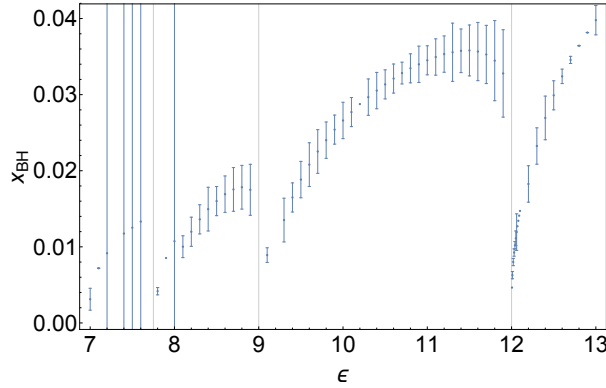


Figure 3.6: Position of the event horizon, x_{BH} , as a function of the field's initial intensity, ϵ . The gaps represent the number of times the field was reflected from spatial infinity before collapsing into a black hole. In this figure the field is reflected from spatial infinity up to three times. The error bars represent the numerical error of the collapse position computed using $2^{14} + 1$ and $2^{15} + 1$ grid points.

find a numerical solution one must pay attention to the error growth. The numerical errors have a huge influence on the δ function, which decreases to very small values with the Π and Φ illusive functions densities, and will influence the CFL condition due to its explicit dependency on the δ function. In this case we can consider small values for the δ function to be of the order of $\delta(t, \pi/2) \simeq -30$.

We were able to compute the time evolution long enough to find that, for large field intensities, $\epsilon \gtrsim 12$, the field does not propagate through space and collapses right away. A detailed observation allows us to notice that, while the intensity decreases, the event horizon also decreases until we reach $x_{BH} = 0$. Proceeding below this point, the field is unable to collapse and is reflected to spatial infinity. At first, one might expect the field to keep propagating back and forth after failure to observe the initial collapse. This is not what is observed, as the field does collapse with a field intensity below the critical point.

In fig. 3.6 one can see the position of the apparent horizon as a function of the field's intensity while in fig. 3.7 presents the time necessary for the field's collapse. We can see in fig. 3.6 that the collapse position is consistent with the literature [5], apart from a numerical factor in the field's initial intensity due to the assumptions made regarding the value of the gravitational constant, G . Furthermore, one may verify that the time of collapse is related to the number of reflections by a factor of π , $T \simeq \pi n_{ref}$, where n_{ref} is the number of reflections at spatial infinity. The error bars presented in the figs. 3.6 and 3.7 do not represent the numerical error regarding an analytical solution, specially because there is no analytical solution, but it does represent the difference between the numerical solutions using different resolutions. We can also observe that the position of the event horizon has a huge error when compared with the error for the time necessary for the field to collapse.

Literature [5] suggests that the critical points follow the law $x_{BH} \propto (\epsilon - \epsilon_0)^\gamma$ with $\gamma = 0.37$. This value will be used as a reference to verify our results' precision. We fit this power law to our results and, from zero to two reflections, the γ function is presented in table 3.1.

These results are not very surprising because the power fit uses the points nearest to the critical intensity and, if one takes a closer look at the positions of the apparent horizon near the critical points,

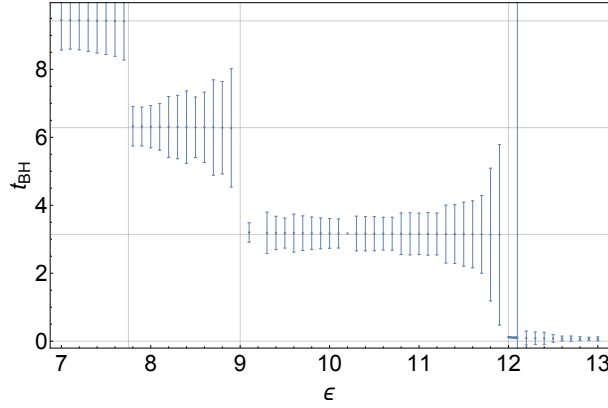


Figure 3.7: Time lapse until field's collapse, t_{BH} , as a function of the field's initial intensity, ϵ . Again, one can see the profiles for the straight collapse and from one to three reflections. The error bars represent the numerical error of the collapse position computed using $2^{14} + 1$ and $2^{15} + 1$ grid points and they represent 100 (one hundred times) the difference between the solutions for the two resolutions.

N_{ref}	ϵ_c	γ	Deviation
0	12.00	0.413	11%
1	9.04	0.426	15%
2	8.04	0.327	12%

Table 3.1: γ values fitting a power function to $x_{BH}(\epsilon)$. These deviations use the literature's value $\gamma = 0.37$ as a reference and they are a result of the difficulty to obtain precise collapse positions near the origin.

one will notice a deviation of the curve's tendency.

After performing several evolutions using small initial intensities, we verified that, for $N = 32679$ points, the evolution doesn't go past $t = 27.6$ or 9 reflections. In any case, the numerical error becomes too large for the system to evolve any further, as the error decreases the value of the δ function at spatial infinity, resulting in $dt \rightarrow 0$. In order to obtain better results, one would have to compute the solutions with more spatial precision and, as a consequence, this would require finer time steps.

We monitored $\Pi^2(t, 0)$, as the curvature is linearly related to this function. We verified, by observing fig. 3.8, that the curvature has almost periodicity π , although this is not entirely true because the δ function influences the speed at which the field propagates and its integral is not constant for all the reflecting cycles. The first fig. of 3.8 seems to validate the results presented in [5], as we see the peaks growing for each iteration.

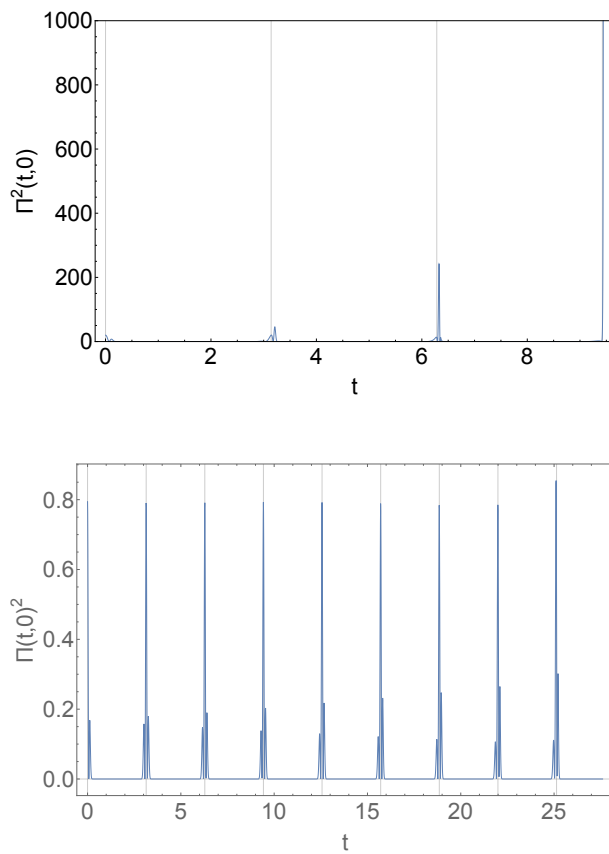


Figure 3.8: Π^2 as a function of time for $\epsilon = 7.0$ and $\epsilon = 1.4$. In these simulations we can see the periodicity of the Π^2 function at the origin. The first simulation did not reach collapse due to numerical errors.

Chapter 4

Conclusions

In this work we studied the evolution of a massless real spherically symmetric scalar field in AdS. We review the developments regarding the dynamics of fields in confined spaces, in particular in AdS spacetimes. We described the ADM formalism, which is used in numerical relativity to obtain the equations that rule the dynamics of a system in GR and, after this, we derived the differential equations that define the evolution of our system along with the proper boundary conditions and asymptotic behaviour of the physical quantities involved. We used a finite difference method to obtain the spatial profiles of the geometric functions and perform some tests in order to verify the convergence of the numerical solutions obtained. After we obtained all the necessary spatial profiles we evolved the scalar field in time, varying the initial field's intensity. We confirmed the literature's description of the collapse mechanism and some of its characteristics. In section 4.1 we will discuss the results we obtained from our simulations and, in section 4.2 we will present some suggestions for future investigation.

4.1 Achievements

We studied some of the properties of the AdS space and motivate a metric that adapts the perturbation caused by the presence of a spherically symmetric scalar field. We present a brief overview of the ADM formalism and how it is possible to derive the dynamic equation of the system. We established the boundary conditions and asymptotic behaviour of the function involved. We also verified that such equations are consistent with the literature [5]. Convergence tests show that the finite difference schemes used to solve the spatial differential equations go asymptotically to the analytical solution on the continuous limit. More elaborate approaches, using higher order derivatives, resulted in a rapid increase of the numerical error in contrast with simpler approaches using a straight forward first derivative finite difference scheme.

After solving numerically the evolution equations we studied the field's collapse as a function of its initial amplitude and we verified that the field always collapsed into a black hole independently of its initial amplitude, at least for $\epsilon > 7$. Beyond that point the numerical error becomes too large, requiring more resolution to study the collapse phenomenon, specially for the apparent horizon position. The

dependency of the collapse time and the black hole horizon, at the moment of the black hole formation, on the initial amplitude as well as the associated numerical errors were also studied. We verified the existence of some critical points, in particular, near $\epsilon = 12$, $\epsilon = 9$ and $\epsilon = 7.75$. Although we just detected these critical points, there probably are an infinite number of critical points associated to the number of reflections at spatial infinity. These critical points are characterized by the collapse position tendency to the $x = 0$, from higher values, and from a gap between collapse positions, from lower values, as the collapse position does not tend to zero from lower field intensities. Unfortunately, the γ values obtained present a large deviation from the results published in the literature and we consider them to be rather inconclusive. This might be a consequence of the acquisition of the event horizon position detection, from a profile equations that use the one-sided spatial derivatives or the number of grid points might be too small to clearly pinpoint the event horizon near the origin. This is a very troublesome task that requires a lot of detail and very long simulations. Furthermore, the curvature at the origin using a small amplitude was also monitored in order to understand its behaviour and how it changes over time. We can see the evolution of the peak curvatures at the origin and its growth supports the results found in the literature stating that the curvature peaks remain constant for the first reflections and tend to grow later during the evolution [5, 21]. In the next section we will discuss some ideas of interest that can be explored in the future.

4.2 Future Work

Although most of our results are in agreement with the literature there are some discrepancies, specially regarding the γ parameter. It would be very useful to be able to accurately pinpoint the collapse position near the origin in order to obtain better values for γ . This could be done either by reconsidering some aspects of the mathematical system, by manipulating some variable computations in the code or using more resolution when near the origin.

The profile studied incorporated the assumption of spherical symmetry. We could drop this symmetry and attempt to simulate a rotating field or other profiles that reveal to be of interest.

The field studied contained only the simplest interaction, the kinematic terms. One could go one step further and explore this field's behaviour under some interactions such as a mass term or with self-interaction or even higher order interactions. As an alternative, one could solve a system consisting in the interaction of two, or more, interacting scalar fields.

Bibliography

- [1] O. Aharony, S. S. Gubser, J. Maldacena, H. Ooguri, and Y. Oz. Large N field theories, string theory and gravity. *Physics Reports*, 323(3):183–386, 2000.
- [2] R. Arnowitt, S. Deser, and C. W. Misner. Dynamical structure and definition of energy in general relativity. *Physical Review*, 116(5):1322, 1959.
- [3] D. Astefanesei and E. Radu. Boson stars with negative cosmological constant. *Nuclear Physics B*, 665:594–622, 2003.
- [4] V. Balasubramanian, A. Buchel, S. R. Green, L. Lehner, and S. L. Liebling. Holographic thermalization, stability of anti-de sitter space, and the fermi-pasta-ulam paradox. *Phys. Rev. Lett.*, 113:071601, Aug 2014.
- [5] P. Bizoń and A. Rostworowski. Weakly Turbulent Instability of Anti-de Sitter Spacetime. *Phys. Rev. Lett.*, 107:031102, Jul 2011.
- [6] A. Buchel, L. Lehner, and S. L. Liebling. Scalar collapse in ads spacetimes. *Phys. Rev. D*, 86:123011, Dec 2012.
- [7] A. Buchel, S. L. Liebling, and L. Lehner. Boson stars in AdS. *arXiv preprint arXiv:1304.4166*, 2013.
- [8] J. Casalderrey-Solana, H. Liu, D. Mateos, K. Rajagopal, and U. A. Wiedemann. Gauge/string duality, hot qcd and heavy ion collisions. *arXiv preprint arXiv:1101.0618*, 2011.
- [9] M. W. Choptuik. Universality and scaling in gravitational collapse of a massless scalar field. *Physical review letters*, 70(1):9, 1993.
- [10] J. Erlich, E. Katz, D. T. Son, and M. A. Stephanov. Qcd and a holographic model of hadrons. *Physical review letters*, 95(26):261602, 2005.
- [11] E. Fermi, J. Pasta, and S. Ulam. Studies of nonlinear problems. 1955.
- [12] D. Garfinkle, C. Cutler, and G. Comer Duncan. Choptuik scaling in six dimensions. *Phys. Rev. D*, 60:104007, Oct 1999.
- [13] D. Garfinkle and L. A. P. Zayas. Rapid thermalization in field theory from gravitational collapse. *Physical Review D*, 84(6):066006, 2011.

- [14] E.ourgoulhon. *3+ 1 Formalism in General Relativity: Bases of Numerical Relativity*, volume 846. Springer, 2012.
- [15] C. Gundlach and J. M. Martín-García. Charge scaling and universality in critical collapse. *Phys. Rev. D*, 54:7353–7360, Dec 1996.
- [16] S. A. Hartnoll. Lectures on holographic methods for condensed matter physics. *Classical and Quantum Gravity*, 26(22):224002, 2009.
- [17] J. Jaluzna, A. Rostworowski, and P. Bizon. AdS collapse of a scalar field in higher dimensions. *Phys. Rev. D*, 84:085021, 2011.
- [18] I. Klebanov. Introduction to the AdS/CFT correspondence. Technical report, 2000.
- [19] J. Maldacena. The large-N limit of superconformal field theories and supergravity. *International journal of theoretical physics*, 38(4):1113–1133, 1999.
- [20] M. Maliborski. Instability of flat space enclosed in a cavity. *arXiv preprint arXiv:1208.2934*, 2012.
- [21] M. Maliborski and A. Rostworowski. Turbulent instability of anti-de sitter space–time. *International Journal of Modern Physics A*, 28(22n23), 2013.
- [22] J. McGreevy. Holographic duality with a view toward many-body physics. *Advances in High Energy Physics*, 2010, 2010.
- [23] H. Okawa. Initial conditions for numerical relativity: Introduction to numerical methods for solving elliptic pdes. *International Journal of Modern Physics A*, 28(22n23):1340016, 2013.
- [24] H. Okawa, V. Cardoso, and P. Pani. On the nonlinear instability of confined geometries. *arXiv preprint arXiv:1409.0533*, 2014.
- [25] P. J. Olver. Numerical analysis lecture notes. 2008.
- [26] F. Pretorius and M. W. Choptuik. Gravitational collapse in 2 + 1 dimensional ads spacetime. *Physical Review D*, 62(12):124012, 2000.
- [27] A. V. Ramallo. Introduction to the AdS/CFT correspondence. *arXiv preprint arXiv:1310.4319*, 2013.
- [28] S. Wolfram. Mathematica, 2014.